ACS OMEGA

http://pubs.acs.org/journal/acsodf

Article

Effect of the Alkyl Chain Length on Assessment as Thermo-Responsive Draw Solutes for Forward Osmosis

Yeonsu Cho and Hyo Kang*

Cite This: *ACS Omega* 2022, 7, 41508−41518

Read Online

ACCESS | Metrics & More | Article Recommendations | Supporting Information

ABSTRACT: A series of thermo-responsive tetrabutylphosphonium 1-alkanesulfonates (abbreviated as $[P_{4444}][C_nS]$, n = 6, 8, 10, and 12), where n is the number of carbon atoms in the alkyl group on the 1-alkanesulfonate anion, were prepared by an ion-exchange reaction to investigate their potential ability toward the application of draw solutes in forward osmosis (FO). We systematically studied the recovery properties and FO performance of $[P_{4444}][C_nS]$. This series exhibited lower critical solution temperature (LCST) characteristics, which offer a clear advantage of being energy-efficient for recovering draw solutes; however, $[P_{4444}][C_6S]$ was only observed at 20 wt %. The LCSTs of the 20 wt % $[P_{4444}][C_6S]$, $[P_{4444}][C_8S]$, $[P_{4444}][C_{10}S]$, and $[P_{4444}][C_{12}S]$ draw solutions were approximately 83, 54, 49, and 56 °C, respectively. Moreover, when the orientation of the active layer was heading toward the draw solution (AL-DS mode), the water and reverse solute flux of $[P_{4444}][C_{10}S]$ were about 1.58 LMH and 0.81 gMH, respectively, at 20 wt % aqueous solutions. When the membrane was used in the active layer facing the feed solution (AL-FS) system, the water and reverse solute flux of $[P_{4444}][C_{10}S]$ were approximately 0.71 LMH and 0.38 gMH, respectively, at 20 wt % aqueous solutions. Thus, this study is the first to examine the structural transformations of the bulkier alkyl group on the sulfonate anion moiety and its feasibility as the new draw solute for the FO system.

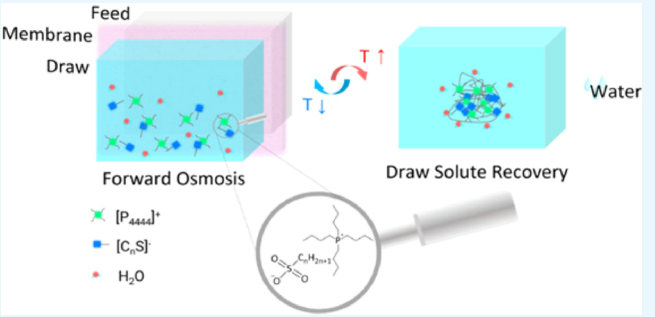

1. INTRODUCTION

With the rapidly growing population, industrialization, and expansion in urbanization, water shortages and energy crises have become some of the most pressing problems worldwide. These problems have led to the development of eco-friendly water treatment techniques. Desalination technologies are universally considered one of the main techniques for producing clean water from a variety of sources and are categorized as thermal or membrane-based processes.[1] Membrane desalination technology has been rapidly developed to clear up the water shortage situation owing to its high efficiency and lower energy consumption than that of thermal desalination technology. Among various membrane processes, reverse osmosis (RO) is the mainly used desalination technology for water treatment.[2,3] However, RO still has an inherent and formidable drawback in that it requires high hydraulic pressures to overcome the force of osmosis generated by the feed source.[4] A variety of alternative technologies for clean water production was proposed and one of them is forward osmosis (FO) desalination which has attracted significant interest as a viable energy-efficient technology.[5−7] FO was operated by the natural osmotic pressure to transport portable water from the feed stream.[8] It could be operated with low or no hydraulic pressure at all, and this technology improves the energy efficiency of clean water production.[9] Compared with pressure-driven RO, osmosis-driven FO has the advantages of low reverse solute flux, minimum environmental impact, low membrane fouling, reversibility of membrane fouling, high water recovery, and low energy intensity.[10,11] FO desalination processes typically consist of two steps: water permeation into the draw solution and water or draw solute recovery from the diluted draw solution. However, several challenges remain in developing a completely feasible FO process. It is important to make the recovery method highly efficient in minimizing the consumed energy and maximizing the recovered draw solute, which in turn maximizes the attained pure water. Thus, the selection of an efficient draw solution is required to obtain low energy costs.[12] The optimal draw solute for FO processes must be chosen, considering its ability not only to induce high osmotic pressure but also to be readily recoverable.

A wide selection of draw solutes with great performance in FO has been proposed over the past few decades, including mixed gases,[13] inorganic salts,[14,15] organic salts,[16−18] nutrient

Received: August 17, 2022
Accepted: October 21, 2022
Published: November 2, 2022

compounds,[19,20] and polyelectrolytes.[18,21,22] Despite the good performance of these draw solutes, their use is limited because of their energy-intensive recovery. To improve draw solute recovery, materials with thermal,[23−27] electric,[28,29] magnetic,[24,30,31] pH-,[32] gas-,[33] and light-[34] responsiveness have been explored. Among these so-called smart materials, thermo-responsive draw solutes have attracted much attention because they can facilitate draw agent reuse and water polishing by heating the spent draw solution.

Thermo-responsive draw solutes show that some aqueous mixtures can undergo dynamic phase transformations upon temperature change.[35−37] There are two special types causing the phase transitions by responding to a temperature change: the upper critical solution temperature (UCST) type and the lower critical solution temperature (LCST) type. In the UCST-type, the aqueous mixture is immiscible below the critical temperature, and the two liquids undergo an increase of miscibility upon heating. Regarding the LCST-type, a homogeneous phase of the aqueous mixture can be changed to a heterogeneous phase upon heating above a specific temperature. Thermo-responsive draw solutes are deemed to be cost-effective because of the possibility of using less expensive and clean energy sources, such as solar or geothermal energy and low-grade waste heat. It may also contribute to eco-friendly FO technology because pure water can be readily attained, and the draw solute can be reused by a change in solution temperature controlled by heating and cooling.

Recently, there has been growing interest in ionic liquids (ILs), which belong to a group of organic salts. They have been considered green solvents and can be applied in catalysis,[38] separation,[39] food,[40] and pharmaceutical processes.[41,42] In addition, ILs are considered optimal choices as draw solutes.[43] First, ILs are composed solely of ions, resulting in high water solubility and ionic strength. Thus, ILs abundantly demonstrate their ability to generate great osmotic force for the movement of fresh water through the FO membrane. In addition, ILs are liquids, which means that their phase separation is significantly faster than that of other thermo-responsive agents, such as polymers. This will also lead to less membrane fouling or flow blocking. ILs are well known as designer solvents which are almost unique to the properties of ILs. A typical IL consists of a hydrophilic or hydrophobic component formed by a combination of cations and anions. The thermo-responsive phase transition can be caused by the hydrophilicity and hydrophobicity balance of the cation and anion at a specific temperature depending on its miscibility in water. Thus, it can be targeted and tailored to the thermo-responsive properties by the interaction balance between the hydrophilic and hydrophobic moieties of the charged components.[36] Hence, thermo-responsive ILs are expected to be promising osmotic agents. Recently, a series of thermo-responsive IL materials have been used to draw solutes for the FO process. The study on the use of an UCST-type IL as the draw solute was taken by Zhong et al.[44] for the first time. The synthesized thermally responsive IL exhibited significant potential as desalination draw solutes, presenting a water-drawing ability capable of dewatering from high saltwater. Cai et al.[23] first investigated a series of LCST-type ILs as draw solutes. These draw solutions can dewater from feed such as brine, with a salinity of 1.6 M NaCl and can be readily regenerated at mild temperatures. Although these thermo-responsive ILs can play a significant role as desalination draw solutes, the findings are still preliminary. Extensive efforts are needed to continuously explore other effective thermo-responsive ILs and systematically investigate their viable application in FO performance.

In this study, we prepared a phosphonium-based monomeric IL series with anions possessing different carbon chains, including 1-hexanesulfonate (C_6S), 1-octanesulfonate (C_8S), 1-decanesulfonate ($C_{10}S$), and 1-dodecanesulfonate ($C_{12}S$), as the draw solutes for FO. The recovery process can be measured by controlling the length of the long alkyl chains. Subsequently, FO performance was thoroughly evaluated to appraise the viability of their application as a draw solute. ILs with LCST behavior were probed for use as draw solutes with low energy consumption. This study provides a promising method to select draw solutes and obtain more scientific information regarding LCST-type ILs in the FO process.

2. EXPERIMENTAL SECTION

2.1. Reagents and Instrumentation. Tetrabutylphosphonium bromide, sodium 1-hexanesulfonate, sodium 1-octanesulfonate, sodium 1-decanesulfonate, and sodium 1-dodecanesulfonate were purchased from Tokyo Chemical Industry (Tokyo, Japan). Dichloromethane and anhydrous magnesium sulfate were obtained from Daejung Chemicals and Metals Co., (Siheung, Republic of Korea). Apple juice (Seoul Milk Company, Seoul, Republic of Korea) and vitamin C (Kyung Nam Pharm Co., Ltd., Seoul, Republic of Korea) were obtained from the local supermarket and pharmacy. All reagents and solvents were not purified anymore, and they were used as received. Distilled water was obtained from Human Power I^+ (Scholar Type, Seoul, Republic of Korea).

The structures of the draw solutes were identified using both MR400 DD2 proton nuclear magnetic resonance (^{1}H NMR; Agilent, USA) and NICOLET iS20 Fourier-transform infrared spectroscopy (FT-IR; Thermo Fisher Scientific, USA). ^{1}H NMR (400 MHz) spectra were collected using a 20 mM solution of the draw solute in deuterated chloroform ($CDCl_3$). Fourier transform infrared (FT-IR) spectroscopy was performed under the attenuated total reflection (ATR) mode over the range of 4000−670 cm^{-1}. The viscosities of the IL samples were determined using a DV-III programmable rheometer (Brookfield, Canada) with rotating a metallic spindle at 85 s^{-1} shear rate. Conductivity was measured using a Seven2Go pro conductivity meter (METTLER TOLEDO, USA). The osmotic pressure of each sample was measured using the freezing point depression method with a K-7400 osmometer (KNAUER, Germany). The LCST behavior was determined by the change in turbidity as a function of temperature using an EMC-11D-V ultraviolet−visible spectrophotometer (UV−vis; λ = 650 nm, EMCLAB Instruments GmbH, Germany) equipped with a TC200P temperature controller (Misung Scientific Co., Ltd., Republic of Korea). Water and reverse solute fluxes were determined by measuring the volumetric change in each solution on both sides of a custom-made U-shaped tube after the experiment. The reverse solute flux was measured by the conductivity change of the feed solution after the experiment using a Seven2Go pro conductivity meter (METTLER TOLEDO, USA).

2.2. Preparation of Tetrabutylphosphonium 1-Hexanesulfonate ($[P_{4444}][C_6S]$), Tetrabutylphosphonium 1-Octanesulfonate ($[P_{4444}][C_8S]$), Tetrabutylphosphonium 1-Decanesulfonate ($[P_{4444}][C_{10}S]$), and Tetrabutylphosphonium 1-Dodecanesulfonate ($[P_{4444}][C_{12}S]$). A mixture

https://doi.org/10.1021/acsomega.2c05279
ACS Omega 2022, 7, 41508−41518

of tetrabutylphosphonium bromide (3.39 g (10 mmol)) and sodium 1-hexanesulfonate (3.76 g (20 mmol)) with a molar ratio of 1:2 was dissolved in distilled water (40 mL) in a 250 mL flat-bottom flask and magnetically stirred at room temperature for 24 h. The product was extracted thrice with dichloromethane and then washed thrice with distilled water to further purify it and then dried over anhydrous $MgSO_4$. Filtration was used to remove the drying agent, and then, the solvent was removed using a rotary evaporator at 50 °C. After evaporation, the remaining solution was further dried overnight in a vacuum at 80 °C, and $[P_{4444}][C_6S]$ was obtained as a viscous IL. $[P_{4444}][C_8S]$, $[P_{4444}][C_{10}S]$, and $[P_{4444}][C_{12}S]$ were prepared using the same method applied when $[P_{4444}][C_6S]$ was prepared, with exception of differing amounts of sodium 1-alkanesulfonate (4.33 g (20 mmol), 4.89 g (20 mmol), and 5.44 g (20 mmol), respectively) and water (40, 135, and 108 mL, respectively) in the mixture. Among them, only the solution-mixed tetrabutylphosphonium bromide and sodium 1-dodecanesulfonate were magnetically stirred at 45 °C.

^{1}H NMR of $[P_{4444}][C_6S]$ [400 MHz, $CDCl_3$, δ/ppm]: 0.79−0.89 (t, 3H, (CH_3−$(CH_2)_3$−CH_2−CH_2−SO_3^-)), 0.90−1.02 (t, 12H, (CH_3−CH_2−CH_2−CH_2−P^+−)), 1.22−1.41 (m, 6H, (CH_3−$(CH_2)_3$−CH_2−CH_2−SO_3^-)), 1.44−1.60 (m, 16H, (CH_3−CH_2−CH_2−CH_2−P^+−)), 1.77−1.91 (m, 2H, (CH_3−$(CH_2)_3$−CH_2−CH_2−SO_3^-)), 2.30−2.45 (t, 8H, (CH_3−CH_2−CH_2−CH_2−P^+−)), 2.76−2.85 (t, 2H, (CH_3−$(CH_2)_3$−CH_2−CH_2−SO_3^-)).

^{1}H NMR of $[P_{4444}][C_8S]$ [400 MHz, $CDCl_3$, δ/ppm]: 0.79−0.89 (t, 3H, (CH_3−$(CH_2)_5$−CH_2−CH_2−SO_3^-)), 0.90−1.02 (t, 12H, (CH_3−CH_2−CH_2−CH_2−P^+−)), 1.16−1.40 (m, 10H, (CH_3−$(CH_2)_5CH_2$−CH_2−SO_3^-)), 1.44−1.59 (m, 16H, (CH_3−CH_2−CH_2−CH_2−P^+−)), 1.76−1.92 (m, 2H, (CH_3−$(CH_2)_5$−CH_2−CH_2−SO_3^-)), 2.27−2.42 (t, 8H, (CH_3−CH_2−CH_2−CH_2−P^+−)), 2.76−2.84 (t, 2H, (CH_3−$(CH_2)_5$−CH_2−CH_2−SO_3^-)).

^{1}H NMR of $[P_{4444}][C_{10}S]$ [400 MHz, $CDCl_3$, δ/ppm]: 0.79−0.89 (t, 3H, (CH_3−$(CH_2)_7$−CH_2−CH_2−SO_3^-)), 0.90−1.02 (t, 12H, (CH_3−CH_2−CH_2−CH_2−P^+−)), 1.16−1.41 (m, 14H, (CH_3−$(CH_2)_7$−CH_2−CH_2−SO_3^-)), 1.43−1.61 (m, 16H, (CH_3−CH_2−CH_2−CH_2−P^+−)), 1.77−1.89 (m, 2H, (CH_3−$(CH_2)_7$−CH_2−CH_2−SO_3^-)), 2.27−2.43 (t, 8H, (CH_3−CH_2−CH_2−CH_2−P^+−)), 2.76−2.85 (t, 2H, (CH_3−$(CH_2)_7$−CH_2−CH_2−SO_3^-)).

^{1}H NMR of $[P_{4444}][C_{12}S]$ [400 MHz, $CDCl_3$, δ/ppm]: 0.81−0.90 (t, 3H, (CH_3−$(CH_2)_9$−CH_2−CH_2−SO_3^-)), 0.91−1.02 (t, 12H, (CH_3−CH_2−CH_2−CH_2−P^+−)), 1.18−1.40 (m, 18H, (CH_3−$(CH_2)_9$−CH_2−CH_2−SO_3^-)), 1.45−1.59 (m, 16H, (CH_3−CH_2−CH_2−CH_2−P^+−)), 1.77−1.94 (m, 2H, (CH_3−$(CH_2)_9$−CH_2−CH_2−SO_3^-)), 2.29−2.42 (t, 8H, (CH_3−CH_2−CH_2−CH_2−P^+−)), 2.76−2.84 (t, 2H, (CH_3−$(CH_2)_9$−CH_2−CH_2−SO_3^-)).

2.3. FO Performance. Water flux is used as a critical indicator to evaluate the FO process performance and has been systematically investigated. As shown in Figure 1, FO measurements were performed in a homemade FO system which consists of two L-shaped glass tubes facing each other. A semipermeable membrane (thin-film composite FO membrane, Hydration Technologies Inc. (HTI)) is a flat-type membrane without mesh spacers and has a diameter of 2.06 cm. The semipermeable membrane was placed between two glass tubes in a channel. The draw and feed solutions were added to each glass tube. The water flux was measured under the active layer facing the draw solution (AL-DS) mode, where the active layer of the semipermeable membrane was in contact with the draw solution and under the active layer facing the feed solution (AL-FS) mode, where the active layer of the semipermeable membrane was in contact with the feed solution. Equal volumes (21 mL) of the draw and feed solutions were concurrently stirred using OCTOPUS CS-4 solenoids (AS ONE, Japan). The water flux was determined from the height difference between each solution in the glass tube after the FO experiment for 20 min. The water flux (J_w, L m^{-2} h^{-1}, LMH) was obtained from the volume increment of the draw solution over time, as shown in eq 1.

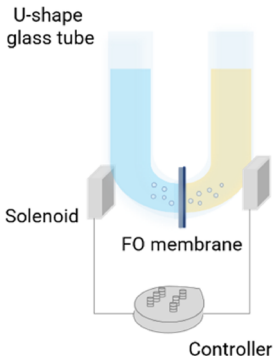

Figure 1. Schematic of the FO set up for permeability investigation of the draw solute.

$$J_w = \frac{\Delta V}{A\Delta T} \quad (1)$$

where ΔV (L), ΔT (h), and A (m^2) denote the volume increase of the draw solution over time ΔT, the FO duration, and the valid area of the membrane (3.32×10^{-4} m^2), respectively.

The reverse solute flux was determined from the quantity of the solute that moved away from the draw solution, and the total dissolved solids (TDS, mg L^{-1}) of the feed solution were measured. Converting the measured conductivity into a concentration is required, based on the conversion factor between the TDS and electrical conductivity (EC, μS cm^{-1}), which is 0.64.[45] The reverse solute flux (J_s, g m^{-2} h^{-1}, gMH) was obtained from the conductivity increment of the feed solution before and after the FO process, as shown in eq 2.

$$J_s = \frac{\Delta(CV)}{A\Delta T} \quad (2)$$

where ΔC (mol L^{-1}), ΔT (h), and ΔV (L) denote the concentration change in the feed solution after time ΔT, the FO duration, and the volume change of the feed solution after time ΔT, respectively.

3. RESULTS AND DISCUSSION

3.1. Preparation and Characterization of $[P_{4444}][C_6S]$, $[P_{4444}][C_8S]$, $[P_{4444}][C_{10}S]$, and $[P_{4444}][C_{12}S]$. The preparative scheme for the tetrabutylphosphonium 1-alkanesulfonate ($[P_{4444}][C_nS]$) series is depicted in Figure 2, which shows that $[P_{4444}][C_6S]$, $[P_{4444}][C_8S]$, $[P_{4444}][C_{10}S]$, and $[P_{4444}][C_{12}S]$ were prepared via anionic exchange of the bromide ion of tetrabutylphosphonium bromide with sodium 1-hexanesulfonate, sodium 1-octanesulfonate, sodium 1-decanesulfonate, and sodium 1-dodecanesulfonate. The chemical structures of the synthesized ionic compounds were identified using ^{1}H NMR and FT-IR spectroscopy.

https://doi.org/10.1021/acsomega.2c05279
ACS Omega 2022, 7, 41508−41518

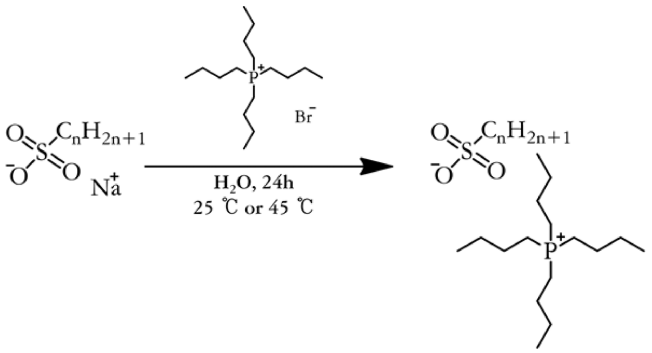

Figure 2. Preparative scheme for tetrabutylphosphonium 1-alkanesulfonate (n = 6, 8, 10, and 12) by the anion exchange reaction.

The ^{1}H NMR spectra of $[P_{4444}][C_6S]$, $[P_{4444}][C_8S]$, $[P_{4444}][C_{10}S]$, and $[P_{4444}][C_{12}S]$ are shown in Figure 3. The ^{1}H NMR spectra clarified the presence of protons from the alkyl group of $[P_{4444}]^+$ (δ = 0.9−1.02 (peak a), 1.43−1.61 (peak b), and 2.27−2.43 (peak c)). The inclusion of the anion moiety in ILs was confirmed by the presence of the alkyl groups of $[C_6S]^-$ (δ = 0.79−0.89 (peak d), 1.22−1.41 (peak e), 1.77−1.91 (peak f), and 2.76−2.85 (peak g)), $[C_8S]^-$ (δ = 0.79−0.89 (peak d), 1.16−1.40 (peak e), 1.76−1.92 (peak f), and 2.76−2.84 (peak g)), $[C_{10}S]^-$ (δ = 0.79−0.89 (peak d), 1.16−1.41 (peak e), 1.77−1.89 (peak f), and 2.76−2.85 (peak g)), and $[C_{12}S]^-$ (δ = 0.81−0.90 (peak d), 1.18−1.40 (peak e), 1.77−1.94 (peak f), and 2.76−2.84 (peak g)). The integrated ratio of each peak area was ideally represented as the ratio of the predicted number of hydrogens that are accountable for each chemical environment. Thus, the ^{1}H NMR spectroscopy results indicated the formation of IL $[P_{4444}][C_6S]$, $[P_{4444}][C_8S]$, $[P_{4444}][C_{10}S]$, and $[P_{4444}][C_{12}S]$, which is supported by the FT-IR spectroscopy results.

Figure 4 shows the FT-IR spectra of ILs $[P_{4444}][C_nS]$ from 4000 to 670 cm^{-1}. The FT-IR spectra of the ILs in this series exhibit three main characteristic peaks. The weak peaks at 699 cm^{-1} were assigned to the vibrations of P−C stretching on the quaternary phosphonium cation.[46] The bands at approximately 1156−1182 and 1028−1034 cm^{-1} could be attributed to the asymmetric and symmetric vibrational stretching of the S═O groups, respectively, in the 1-alkane sulfonate anion.[47] Consequently, we identified the presence of $[P_{4444}]^+$, $[C_6S]^-$, $[C_8S]^-$, $[C_{10}S]^-$, and $[C_{12}S]^-$ by the characteristic IR peaks of the functional groups such as the S═O bond on the 1-alkane sulfonate anion and the P−C bond on the quaternary phosphonium cation. Thus, the spectroscopic results prove that IL $[P_{4444}][C_6S]$, $[P_{4444}][C_8S]$, $[P_{4444}][C_{10}S]$, and $[P_{4444}][C_{12}S]$ were successfully prepared.

3.2. Viscosity. Low viscosity is one of the main factors for ideal draw solution because it affects the efficiency of the FO process. When the draw solution viscosity was increased, increasing severity of internal concentration polarization (ICP) or external concentration polarization (ECP) phenomena could arise on the membrane, which result in the low water flux value. As shown in Figure 5, the viscosity of $[P_{4444}][C_6S]$ was approximately 1.40, 1.68, 1.76, and 1.96 cP, at 5, 10, 15, and 20 wt %, respectively. It is observed that the viscosity of the $[P_{4444}][C_nS]$ series increases with the increase in the concentration. Also, when a concentration of draw solution is 20 wt %, viscosities of $[P_{4444}][C_6S]$, $[P_{4444}][C_8S]$, $[P_{4444}][C_{10}S]$, and $[P_{4444}][C_{12}S]$ were approximately 1.96, 2.72, 3.72, and 4.32 cP, respectively. The viscosity of the draw solutions show the order of $[P_{4444}][C_{12}S]$ > $[P_{4444}][C_{10}S]$ >

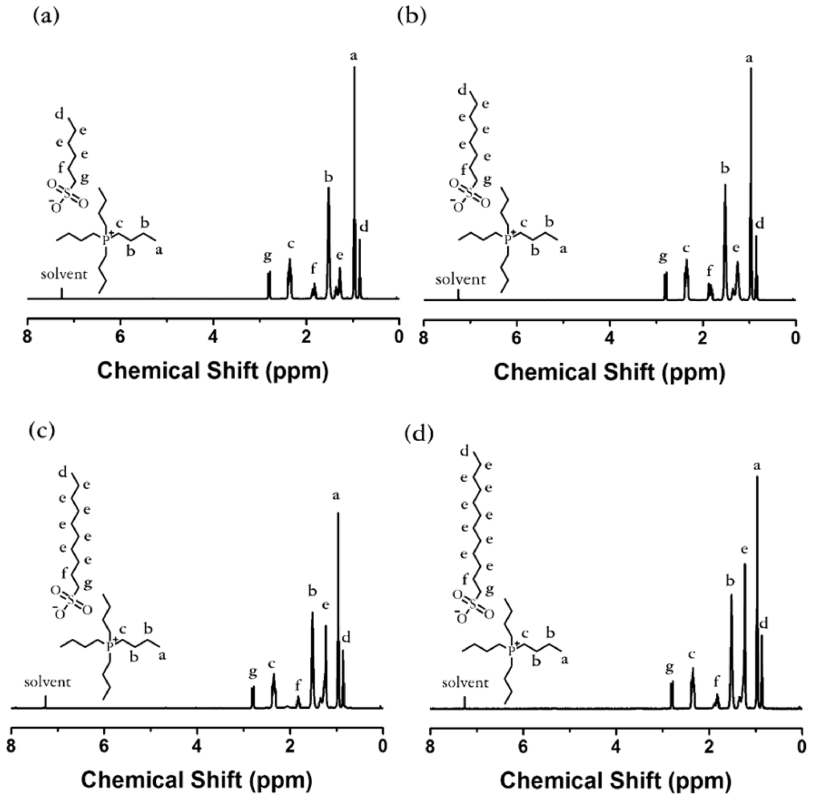

Figure 3. Proton ^{1}H NMR spectra of (a) $[P_{4444}][C_6S]$, (b) $[P_{4444}][C_8S]$, (c) $[P_{4444}][C_{10}S]$, and (d) $[P_{4444}][C_{12}S]$.

https://doi.org/10.1021/acsomega.2c05279
ACS Omega 2022, 7, 41508−41518

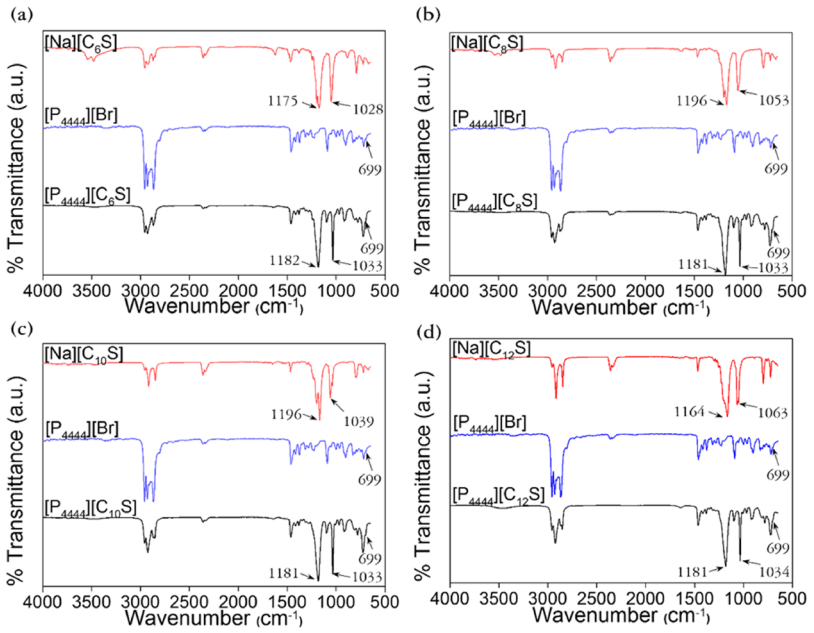

Figure 4. FT-IR spectra of (a) $[P_{4444}][C_6S]$, (b) $[P_{4444}][C_8S]$, (c) $[P_{4444}][C_{10}S]$, and (d) $[P_{4444}][C_{12}S]$.

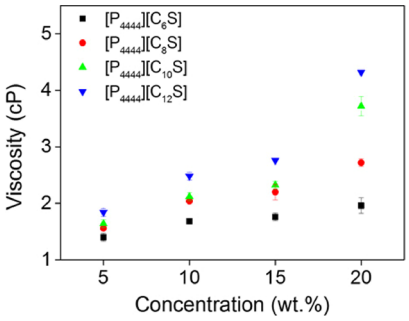

Figure 5. Viscosities of $[P_{4444}][C_nS]$ IL series according to the solution concentration.

$[P_{4444}][C_8S] > [P_{4444}][C_6S]$. The reason is that the increase in alkyl chain lengths leads to a rise in van der Waals interactions, thereby increasing the viscosity values.[48] Accordingly, $[P_{4444}][C_6S]$ having the shortest alkyl chain in the series can induce low viscosity.

3.3. Electrical Conductivity. Electrical conductivity is an intrinsic property of a material that is related to the electrical activity of a material that can carry electricity.[49−51] Factors related to the better generation of electrical conductivity, ion activity, and ion mobility are considered, which means that the solutes are well dissociated in water.[52,53] The electrical conductivity of the $[P_{4444}][C_nS]$ series is shown as a function of the concentration in Figure 6. For example, the electrical conductivities of $[P_{4444}][C_6S]$ were approximately 3235, 4942,

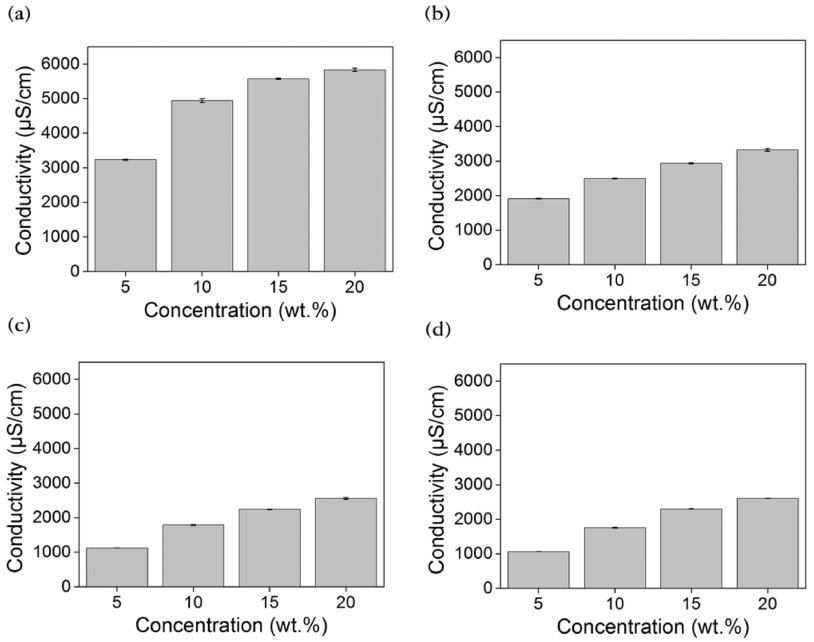

Figure 6. Conductivity of (a) $[P_{4444}][C_6S]$, (b) $[P_{4444}][C_8S]$, (c) $[P_{4444}][C_{10}S]$, and (d) $[P_{4444}][C_{12}S]$ according to the solution concentration.

https://doi.org/10.1021/acsomega.2c05279
ACS Omega 2022, 7, 41508−41518

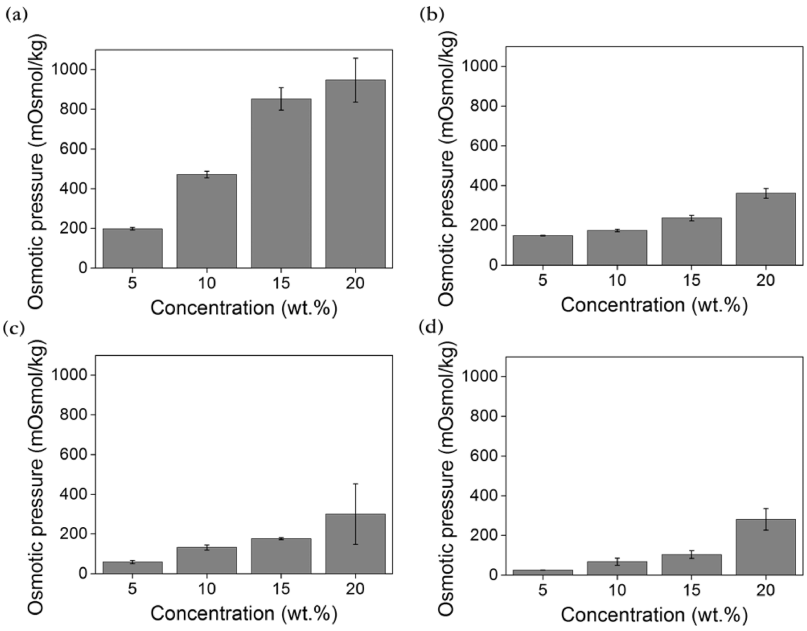

Figure 7. Osmotic pressure of (a) $[P_{4444}][C_6S]$, (b) $[P_{4444}][C_8S]$, (c) $[P_{4444}][C_{10}S]$, and (d) $[P_{4444}][C_{12}S]$ according to the solution concentration.

5574, and 5831 μS cm^{-1} at 5, 10, 15, and 20 wt %, respectively. This result indicates that the electrical conductivity exhibited an increasing trend as the draw solute concentration increased.

When the concentration was 20 wt %, the conductivities of $[P_{4444}][C_6S]$, $[P_{4444}][C_8S]$, $[P_{4444}][C_{10}S]$, and $[P_{4444}][C_{12}S]$ were found to be approximately 5831, 3327, 2559, and 2607 μS cm^{-1}, respectively. The electrical conductivity decreased with elongating the alkyl chain length, that is, the electrical conductivity of the draw solutions followed the order of $[P_{4444}][C_6S] > [P_{4444}][C_8S] > [P_{4444}][C_{10}S] > [P_{4444}][C_{12}S]$. Increasing the alkyl chain length led to a noticeable decrease in electrical conductivity, indicating poor ion activity and mobility, as increasing the bulkiness of the alkyl group is expected to hinder ion mobility. These trends of the electrical conductivity are similar to those of the osmotic pressure upon increasing the concentration of the IL solution and varying the alkyl chain length in the structure of the draw solute, as will be discussed later.

3.4. Osmotic Pressure. The osmotic pressure difference between two solutions, that is to say, draw and feed solution, is indicative of water permeability. A higher osmotic pressure gradient can yield better flux performance and can be satisfied when a draw solution and feed solution possess a higher osmotic pressure and a lower osmotic pressure, respectively. The osmotic pressure (π) can be calculated through the van't Hoff equation (eq 3), as shown below, and its concentration dependence can also be seen.[54]

$$\pi = C_i RT \tag{3}$$

where π denotes the osmotic pressure, C_i the molar concentration of solute i, R the universal gas constant, and T the temperature (K).

The osmotic pressure was measured using the freezing point depression method at different concentrations, that is, 5, 10, 15, and 20 wt %, to evaluate the feasibility of $[P_{4444}][C_6S]$, $[P_{4444}][C_8S]$, $[P_{4444}][C_{10}S]$, and $[P_{4444}][C_{12}S]$ as a new draw solute.

As shown in Figure 7, at 5, 10, 15, and 20 wt %, the osmotic pressures of $[P_{4444}][C_6S]$ were approximately 199, 472, 852, and 947 mOsmol/kg, respectively. For all draw solutes, this result exhibits an increasing trend as an increase in the IL concentration. The osmotic pressure is a colligative property, which means that it is dependent on the concentration of solute particles in solution, and it has an increasing trend with an increase in concentration, as expected. However, a long alkyl chain on anion of this $[P_{4444}][C_nS]$ IL series is similar to structures of hydrophobic surfactants, and thus, $[P_{4444}][C_nS]$ IL series may be not fully dissolved in water. According to the previous study,[55−57] the formation of micelle-like aggregates reduces the number of free ILs, thereby resulting in the osmotic pressures of the IL aqueous solutions becoming lower than that predicted from the van't Hoff theory. Therefore, it can be considered that osmotic pressures of the $[P_{4444}][C_nS]$ IL molecules may be unfit to van't Hoff theory in the high concentration range because of a reduction in the number of free ILs by micelle formation. At a concentration of 20 wt %, the osmotic pressures of $[P_{4444}][C_6S]$, $[P_{4444}][C_8S]$, $[P_{4444}][C_{10}S]$, and $[P_{4444}][C_{12}S]$ were approximately 947, 362, 301, and 281 mOsmol/kg, respectively. Analogous to the trend in the electrical conductivity, the result exhibits a decreasing tendency of osmotic pressure with increasing the carbon number of the alkyl chain on the anion part of the ILs. This result is related to the role of the hydrophobic segment, which is attributed to the generation of freely hydrated ions; thus, the hydrophobic segment can cause a decrease in solubility in an aqueous state.[23,36,58,59] The long alkyl chains on the sulfonate group are hydrophobic segments that generate less osmotic pressure in an aqueous mixture. Therefore, the short alkyl chain exhibited a weak degree of hydrophobicity, resulting in $[P_{4444}][C_6S]$ having the highest osmotic pressure. $[P_{4444}][C_{12}S]$, which has the longest alkyl chain in the series, can induce severely low osmotic pressures.

3.5. Recovery Properties. The recovery property is vital to achieving the feasible FO, which helps ease regeneration to improve energy efficiency for water recovery and draw solute regeneration in the FO. A LCST is a type of thermally induced phase transition in which a homogeneous IL solution is formed in the separated phases upon a gradual increase in the

https://doi.org/10.1021/acsomega.2c05279
ACS Omega 2022, 7, 41508−41518

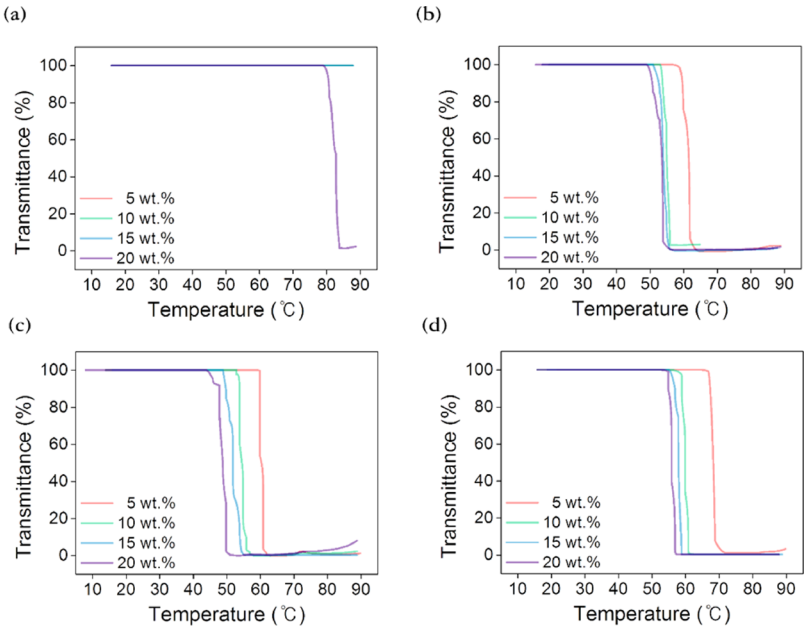

Figure 8. LCST behavior of (a) $[P_{4444}][C_6S]$, (b) $[P_{4444}][C_8S]$, (c) $[P_{4444}][C_{10}S]$, and (d) $[P_{4444}][C_{12}S]$ according to the solution concentration.

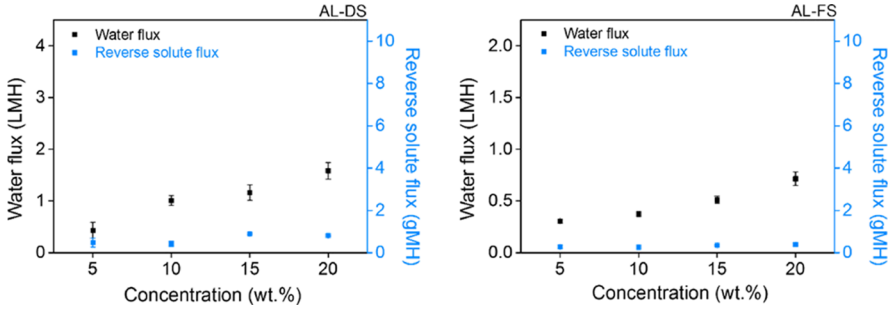

Figure 9. Water flux and reverse solute flux of $[P_{4444}][C_{10}S]$ in AL-DS (left) and AL-FS (right).

temperature of the IL solution. Materials exhibiting LCST properties are attractive and good for use as drawing agents because they can be separated from the spent draw solution by only heating; these LCST properties were attributed to the efficient water recovery and draw solute regeneration. In an aqueous solution, LCST measurements of $[P_{4444}][C_6S]$, $[P_{4444}][C_8S]$, $[P_{4444}][C_{10}S]$, and $[P_{4444}][C_{12}S]$ were conducted using UV−vis spectroscopy equipped with a temperature controller. The temperature at 50% transmittance was defined as the LCST phase-transition temperature by the transmittance curve changed upon temperature change.

As can be observed in Figure 8, when their aqueous solution was the concentration of 10 wt %, the LCST of $[P_{4444}][C_6S]$ is not shown within the entire analyzed temperature range and those of $[P_{4444}][C_8S]$, $[P_{4444}][C_{10}S]$, and $[P_{4444}][C_{12}S]$ were approximately 55, 55, and 56 °C, respectively. At a concentration of 20 wt %, the LCSTs were manifested at 83 °C and also decreased to 54, 49, and 56 °C, respectively. The LCST property is basically provided by hydrophobic hydration, and this behavior has a reasonably comprehensible viewpoint concerning the relationship between temperature and draw solute solubility in an aqueous state.[36,58,59] Below the LCST of ILs, $[P_{4444}][C_6S]$, $[P_{4444}][C_8S]$, $[P_{4444}][C_{10}S]$, and $[P_{4444}][C_{12}S]$ exist as free ILs in solution because of the formation of intensive H-bonding with water molecules. The protons on the alkyl moieties of the quaternary phosphonium cation and the 1-alkanesulfonate anion of $[P_{4444}][C_6S]$, $[P_{4444}][C_8S]$, $[P_{4444}][C_{10}S]$, and $[P_{4444}][C_{12}S]$ can accept the oxygen lone pairs in water. When heated above the LCST of ILs, $[P_{4444}][C_6S]$, $[P_{4444}][C_8S]$, $[P_{4444}][C_{10}S]$, and $[P_{4444}]$-$[C_{12}S]$ formed stronger ion-ion interactions, which were between the $[P_{4444}]^+$ and $[C_6S]^-$, $[C_8S]^-$, $[C_{10}S]^-$, and $[C_{12}S]^-$, than those of the IL−water interactions, which can lead to aggregation and the formation of heterogeneous phases in aqueous solutions. Interestingly, the LCST tendency of the four draw solutes decreased with increasing carbon number, that is, *n*, except for the draw solute with 12 carbon atoms ($[P_{4444}][C_{12}S]$). The LCST characteristics with $[P_{4444}][C_nS]$ draw solutions follows the order of $[P_{4444}][C_6S]$ > $[P_{4444}]$-$[C_{12}S]$ > $[P_{4444}][C_8S]$ > $[P_{4444}][C_{10}S]$. It is also noteworthy that the LCST measurements revealed that the phase-transition temperature did not exhibit a linear relationship with the hydrophobic alkyl chain length. Hence, an appropriate LCST in the $[P_{4444}][C_nS]$ series was observed for the alkyl chain length of 10 carbon atoms. This result may be related, in part, to the IL−IL interaction, which consists of van der Waals and electrostatic interactions. The van der Waals interaction between ILs would be strong owing to the increased surface area of the molecule, whereas the ionic interaction between ILs would be weak with increasing alkyl chain lengths.[60] It can be inferred that modulating the alkyl chain length can tune the LCST behavior by their interactions with each other, which is a

https://doi.org/10.1021/acsomega.2c05279
ACS Omega 2022, 7, 41508−41518

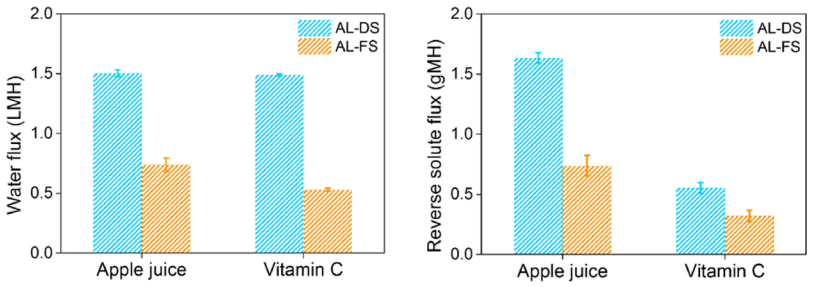

Figure 10. Water flux (left) and reverse solute flux (right) of the FO process with apple juice and vitamin C solution as feed solutions under room temperature.

competitive relationship between van der Waals and electrostatic interactions. Thus, it is interesting to observe that the two interactions between the ILs are optimally balanced in the IL $[P_{4444}][C_{10}S]$. These results indicate that the LCST properties could be tuned by modulating the length of the hydrophobic alkyl chains. The additional experimental data for the phase transition temperature according to various concentrations are provided in the Supporting information (see Figure S1).

3.6. Water and Reverse Solute Fluxes. Water and reverse fluxes were measured to see if the draw solute has great performance for FO goal of becoming the eco-friendly desalination technology. The FO measurement was systematically performed using $[P_{4444}][C_{10}S]$ as the draw solute because it had the lowest LCST in this series. The FO process was performed in the AL-DS and AL-FS modes using custom-made glass tubes. Each side of the two connecting glass tubes was filled with draw solutions of various concentrations, that is, 5, 10, 15, and 20 wt % aqueous solutions of $[P_{4444}][C_{10}S]$ and distilled water as the feed solution, respectively. The instrument was placed at room temperature, which was below the LCST of $[P_{4444}][C_{10}S]$.

Figure 9 shows that the water flux of $[P_{4444}][C_{10}S]$ was measured to be approximately 0.43, 1.00, 1.16, and 1.58 LMH at 5, 10, 15, and 20 wt % under the AL-DS mode, respectively. As against water flux value under the AL-DS mode, that of $[P_{4444}][C_{10}S]$ was measured as about 0.31, 0.37, 0.51, and 0.71 LMH at a low value under the AL-FS mode, respectively. These results indicated that the increasing trend of $[P_{4444}][C_{10}S]$ was more prominent in the AL-DS mode than in the AL-FS mode. This is associated with the absence of dilutive ICP as the draw solution is in direct contact with the active layer.[61,62] The AL-DS mode did not suffer from concentrative ICP owing to the use of distilled water as feed. Therefore, the overall effective osmotic pressure gradient ($\Delta\pi_{eff}$) was higher than that in the AL-FS mode, leading to higher water flux values in the AL-DS mode. The concentration of the draw solution is a factor that significantly influences FO performance. Its reason is that a high concentration of the draw solution could induce a high osmotic pressure to improve water flux. As expected, the water flux of $[P_{4444}][C_{10}S]$ improved with increasing concentration in AL-DS and AL-FS modes. Additionally, with water permeation, a desirable draw solute must leak toward the feed solution across the membrane by the draw solute concentration difference. Draw solute leakage is reflected in the reverse solute flux value, which has detrimental effects such as gradual loss of the draw solute, reduced osmotic driving force (that is, low water flux), severe fouling phenomena, and elevated operating costs owing to periodic replenishment of the draw solute.

The reverse solute flux was observed at 5, 10, 15, and 20 wt % of the $[P_{4444}][C_{10}S]$ draw solution as between 0.42 and 0.89 gMH and between 0.26 and 0.38 gMH under AL-DS and AL-FS modes, respectively. For both operation modes, $[P_{4444}][C_{10}S]$ exhibited a low reverse solute flux. Direct contact between the active layer and the draw solution was favorable for reverse solute movement owing to a higher effective osmotic pressure gradient ($\Delta\pi_{eff}$), compared to AL-FS mode.[63,64] Because of the concentration polarization (CP) phenomenon, the reverse solute flux was high in the AL-DS mode, compared to the value achieved in the AL-FS mode.

3.7. Food/Beverage and Pharmaceutical Concentration Performance and Recycling Study. For long shelf life and stable product quality, commercial foodstuff and pharmaceutical product, which contain beneficial nutrition for human health such as vitamins, minerals, and so on, are generally concentrated by removing water.[5,65] To show applicability in the field of food/beverage and pharmaceutical concentration, the $[P_{4444}][C_{10}S]$ could be performed with various feeds such as foodstuff and pharmaceutical products. The food/beverage and pharmaceutical concentration performance were measured using 20 wt % solution of $[P_{4444}][C_{10}S]$ as a draw solution and apple juice and vitamin C in an aqueous solution as a feed solution. As shown in Figure 10, when using apple juice and vitamin C solution, the water permeation fluxes were approximately 1.50 and 1.49 LMH under the AL-DS mode, respectively. Under the AL-FS mode, the respective water permeation fluxes were approximately 0.74 and 0.53 LMH. This application performance results clearly state that the $[P_{4444}][C_{10}S]$ draw solute system has the possibility to utilize it for food and pharmaceutical concentrations.

To evaluate the recycling ability of $[P_{4444}][C_{10}S]$ which is directly related to the FO efficiency, the osmotic pressures and LCST behaviors of $[P_{4444}][C_{10}S]$ were measured at 20 wt % concentration after repeatedly operating FO using distilled water as a feed solution and thermal recovery step. As shown in Figure 11, the 20 wt % $[P_{4444}][C_{10}S]$ solution whose osmotic pressures slightly decrease from 298.33 to 295.67 mOsmol/kg has very similar osmotic pressure values after the 4th FO run in comparison with the first FO run. However, the LCST value of the 20 wt % $[P_{4444}][C_{10}S]$ solution slightly increases from 49 to 50 °C after the fourth FO run. This recycling result clearly shows that the $[P_{4444}][C_{10}S]$ draw solute could achieve the actual feasibility to reuse it for water treatment with very few property transformation.

4. CONCLUSIONS

A series of thermo-responsive ILs tetrabutylphosphonium 1-alkanesulfonates, $[P_{4444}][C_nS]$, where n is the number of

https://doi.org/10.1021/acsomega.2c05279
ACS Omega 2022, 7, 41508−41518

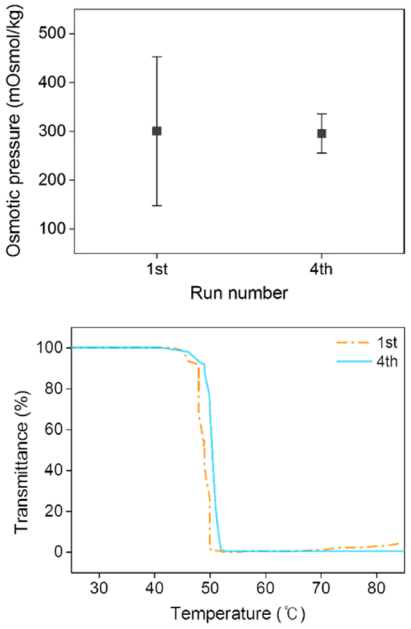

Figure 11. Osmotic pressures (top) and LCST behavior (bottom) of $[P_{4444}][C_{10}S]$ after the repeated FO runs using distilled water as a feed solution.

carbon atoms in the alkyl group, was synthesized to examine its capability of optimal candidates as a draw solute in FO. The $[P_{4444}][C_nS]$ series exhibited LCST characteristics, but $[P_{4444}][C_6S]$ only exhibited LCST characteristics at a 20 wt % concentration. At a 20 wt % concentration, the LCSTs of $[P_{4444}][C_6S]$, $[P_{4444}][C_8S]$, $[P_{4444}][C_{10}S]$, and $[P_{4444}][C_{12}S]$ were 83, 54, 49, and 56 °C, respectively, which show bright prospects in the application of the draw solute for the low-energy recovery step. Furthermore, these results indicate that the LCSTs appear in the order of $[P_{4444}][C_{10}S]$, $[P_{4444}][C_8S]$, $[P_{4444}][C_{12}S]$, and $[P_{4444}][C_6S]$. $[P_{4444}][C_{10}S]$ had the lowest LCST among all the draw solutes, indicating that it is promising to utilize $[P_{4444}][C_{10}S]$ as a draw solute in this series. Because the recovery temperature was near room temperature, the energy efficiency for recovering the draw solute was greater. The water flux of $[P_{4444}][C_{10}S]$ was calculated as nearly 1.65 and 0.74 LMH at 20 wt % under two modes shifted by the active layer orientation (AL-DS and AL-FS mode), respectively, and the respective reverse solute fluxes were 0.78 and 0.35 gMH under the same conditions. The novelty of this study included that we first conduct the development of this material, which contributes to expanding the selection of IL and this study has done much to advance the knowledge in the material science field. Especially, this study provides inspiration for the effect of the bulkier alkyl group modification on the ability to draw solutes and a notable finding for designing potentially regenerable draw solutes. The $[P_{4444}][C_{10}S]$ IL also shows great promise as the FO draw solute along with the advantage of a simply accessible synthesis method and the impact on FO efficiencies with low recovery temperatures.

■ ASSOCIATED CONTENT

Supporting Information

The Supporting Information is available free of charge at https://pubs.acs.org/doi/10.1021/acsomega.2c05279.

LCST-type phase diagram of $[P_{4444}][C_nS]$ IL series in aqueous solution according to various concentrations (PDF)

■ AUTHOR INFORMATION

Corresponding Author

Hyo Kang − *BK-21 Four Graduate Program, Department of Chemical Engineering, Dong-A University, Busan 49315, Republic of Korea;* orcid.org/0000-0002-0297-7216; Phone: +82 51 200 7720; Email: hkang@dau.ac.kr; Fax: +82 51 200 7728

Author

Yeonsu Cho − *BK-21 Four Graduate Program, Department of Chemical Engineering, Dong-A University, Busan 49315, Republic of Korea*

Complete contact information is available at: https://pubs.acs.org/10.1021/acsomega.2c05279

Notes

The authors declare no competing financial interest.

■ ACKNOWLEDGMENTS

Financial support by the Dong-A University Research Fund is gratefully acknowledged.

■ REFERENCES

(1) Cohen, Y.*Advances in Water Desalination Technologies*; World Scientific: Singapore2021.

(2) Prihasto, N.; Liu, Q.; Kim, S. Pre-treatment strategies for seawater desalination by reverse osmosis system. *Desalination* **2009**, *249*, 308−316.

(3) Wang, X.; Liu, Y.; Pan, X.; Han, J.; Hao, J. Parameters for seawater reverse osmosis product water: a review. *Exposure Health* **2017**, *9*, 157−168.

(4) Greenlee, L. F.; Lawler, D. F.; Freeman, B. D.; Marrot, B.; Moulin, P. Reverse osmosis desalination: Water sources, technology, and today's challenges. *Water Res.* **2009**, *43*, 2317−2348.

(5) Haupt, A.; Lerch, A. Forward osmosis application in manufacturing industries: A short review. *Membranes* **2018**, *8*, 47.

(6) Mohammadifakhr, M.; de Grooth, J.; Roesink, H. D.; Kemperman, A. J. Forward osmosis: A critical review. *Processes* **2020**, *8*, 404.

(7) Suwaileh, W.; Pathak, N.; Shon, H.; Hilal, N. Forward osmosis membranes and processes: A comprehensive review of research trends and future outlook. *Desalination* **2020**, *485*, No. 114455.

(8) Cath, T. Y.; Childress, A. E.; Elimelech, M. Forward osmosis: Principles, applications, and recent developments. *J. Membr. Sci.* **2006**, *281*, 70−87.

(9) Akther, N.; Sodiq, A.; Giwa, A.; Daer, S.; Arafat, H. A.; Hasan, S. W. Recent advancements in forward osmosis desalination: A review. *Chem. Eng. J.* **2015**, *281*, 502−522.

(10) Ibrar, I.; Altaee, A.; Zhou, J. L.; Naji, O.; Khanafer, D. Challenges and potentials of forward osmosis process in the treatment of wastewater. *Crit. Rev. Environ. Sci. Technol.* **2020**, *50*, 1339−1383.

(11) Wang, J.; Liu, X. Forward osmosis technology for water treatment: Recent advances and future perspectives. *J. Cleaner Prod.* **2021**, *280*, No. 124354.

(12) Long, Q.; Jia, Y.; Li, J.; Yang, J.; Liu, F.; Zheng, J.; Yu, B. Recent advance on draw solutes development in forward osmosis. *Processes* **2018**, *6*, 165.

(13) McCutcheon, J. R.; McGinnis, R. L.; Elimelech, M. A novel ammonia—carbon dioxide forward (direct) osmosis desalination process. *Desalination* **2005**, *174*, 1−11.

(14) Achilli, A.; Cath, T. Y.; Childress, A. E. Selection of inorganic-based draw solutions for forward osmosis applications. *J. Membr. Sci.* **2010**, *364*, 233−241.
(15) Chekli, L.; Kim, Y.; Phuntsho, S.; Li, S.; Ghaffour, N.; Leiknes, T.; Shon, H. K. Evaluation of fertilizer-drawn forward osmosis for sustainable agriculture and water reuse in arid regions. *J. Environ. Manage.* **2017**, *187*, 137−145.
(16) Stone, M. L.; Wilson, A. D.; Harrup, M. K.; Stewart, F. F. An initial study of hexavalent phosphazene salts as draw solutes in forward osmosis. *Desalination* **2013**, *312*, 130−136.
(17) Ge, Q.; Fu, F.; Chung, T. Ferric and cobaltous hydroacid complexes for forward osmosis (FO) processes. *Water Res.* **2014**, *58*, 230−238.
(18) Huang, J.; Long, Q.; Xiong, S.; Shen, L.; Wang, Y. Application of poly (4-styrenesulfonic acid-co-maleic acid) sodium salt as novel draw solute in forward osmosis for dye-containing wastewater treatment. *Desalination* **2017**, *421*, 40−46.
(19) Kravath, R. E.; Davis, J. A. Desalination of sea water by direct osmosis. *Desalination* **1975**, *16*, 151−155.
(20) Ng, H. Y.; Tang, W. Forward (direct) osmosis: A novel and prospective process for brine control. *Proc. Water Environ. Fed.* **2006**, *2006*, 4345−4352.
(21) Ge, Q.; Su, J.; Amy, G. L.; Chung, T. Exploration of polyelectrolytes as draw solutes in forward osmosis processes. *Water Res.* **2012**, *46*, 1318−1326.
(22) Ge, Q.; Wang, P.; Wan, C.; Chung, T. Polyelectrolyte-promoted forward osmosis-membrane distillation (FO-MD) hybrid process for dye wastewater treatment. *Environ. Sci. Technol.* **2012**, *46*, 6236−6243.
(23) Cai, Y.; Shen, W.; Wei, J.; Chong, T. H.; Wang, R.; Krantz, W. B.; Fane, A. G.; Hu, X. Energy-efficient desalination by forward osmosis using responsive ionic liquid draw solutes. *Environ. Sci.: Water Res. Technol.* **2015**, *1*, 341−347.
(24) MingáLing, M. Facile synthesis of thermosensitive magnetic nanoparticles as "smart" draw solutes in forward osmosis. *Chem. Commun.* **2011**, *47*, 10788−10790.
(25) Ju, C.; Kang, H. Zwitterionic polymers showing upper critical solution temperature behavior as draw solutes for forward osmosis. *RSC Adv.* **2017**, *7*, 56426−56432.
(26) Inada, A.; Takahashi, T.; Kumagai, K.; Matsuyama, H. Morpholine derivatives as thermoresponsive draw solutes for forward osmosis desalination. *Ind. Eng. Chem. Res.* **2019**, *58*, 12253−12260.
(27) Abdullah, M. A. M.; Man, M. S.; Abdullah, S. B.; Saufi, S. M. A glance on thermo-responsive ionic liquids as draw solution in forward osmosis system. *Desalin. Water Treat.* **2020**, *206*, 165−176.
(28) Zhang, H.; Li, J.; Cui, H.; Li, H.; Yang, F. Forward osmosis using electric-responsive polymer hydrogels as draw agents: Influence of freezing−thawing cycles, voltage, feed solutions on process performance. *Chem. Eng. J.* **2015**, *259*, 814−819.
(29) Cui, H.; Zhang, H.; Yu, M.; Yang, F. Performance evaluation of electric-responsive hydrogels as draw agent in forward osmosis desalination. *Desalination* **2018**, *426*, 118−126.
(30) Ling, M. M.; Wang, K. Y.; Chung, T. Highly water-soluble magnetic nanoparticles as novel draw solutes in forward osmosis for water reuse. *Ind. Eng. Chem. Res.* **2010**, *49*, 5869−5876.
(31) Ge, Q.; Su, J.; Chung, T.; Amy, G. Hydrophilic super-paramagnetic nanoparticles: synthesis, characterization, and performance in forward osmosis processes. *Ind. Eng. Chem. Res.* **2011**, *50*, 382−388.
(32) Cai, Y.; Shen, W.; Wang, R.; Krantz, W. B.; Fane, A. G.; Hu, X. CO 2 switchable dual responsive polymers as draw solutes for forward osmosis desalination. *Chem. Commun.* **2013**, *49*, 8377−8379.
(33) Stone, M. L.; Rae, C.; Stewart, F. F.; Wilson, A. D. Switchable polarity solvents as draw solutes for forward osmosis. *Desalination* **2013**, *312*, 124−129.
(34) Han, H.; Lee, J. Y.; Lu, X. Thermoresponsive nanoparticles plasmonic nanoparticles = photoresponsive heterodimers: Facile synthesis and sunlight-induced reversible clustering. *Chem. Commun.* **2013**, *49*, 6122−6124.
(35) Saita, S.; Mieno, Y.; Kohno, Y.; Ohno, H. Ammonium based zwitterions showing both LCST-and UCST-type phase transitions after mixing with water in a very narrow temperature range. *Chem. Commun.* **2014**, *50*, 15450−15452.
(36) Kohno, Y.; Saita, S.; Men, Y.; Yuan, J.; Ohno, H. Thermoresponsive polyelectrolytes derived from ionic liquids. *Polym. Chem.* **2015**, *6*, 2163−2178.
(37) Pang, B.; Yu, Y.; Zhang, W. Thermoresponsive Polymers Based on Tertiary Amine Moieties. *Macromol. Rapid Commun.* **2021**, *42*, No. 2100504.
(38) Steinrueck, H.; Wasserscheid, P. Ionic liquids in catalysis. *Catal. Lett.* **2015**, *145*, 380−397.
(39) Flieger, J.; Grushka, E. B.; Czajkowska-Zelazko, A. Ionic liquids as solvents in separation processes. *Austin J. Anal. Pharm. Chem.* **2014**, *1*, 1009.
(40) Toledo Hijo, A. A.; Maximo, G. J.; Costa, M. C.; Batista, E. A.; Meirelles, A. J. Applications of ionic liquids in the food and bioproducts industries. *ACS Sustainable Chem. Eng.* **2016**, *4*, 5347−5369.
(41) Shamshina, J. L.; Berton, P.; Wang, H.; Zhou, X.; Gurau, G.; Rogers, R. D.Ionic liquids in pharmaceutical industry. In *Green techniques for organic synthesis and medicinal chemistry*, 2nd ed.; Zhang, W, Cue, B.W., Eds.; Wiley: New York, 2018; pp 539−577.
(42) Pedro, S. N.; Freire, C. S. R.; Silvestre, A. J.; Freire, M. G. The role of ionic liquids in the pharmaceutical field: An overview of relevant applications. *Int. J. Mol. Sci.* **2020**, *21*, 8298.
(43) Dutta, S.; Nath, K. Prospect of ionic liquids and deep eutectic solvents as new generation draw solution in forward osmosis process. *J. Water Process Eng.* **2018**, *21*, 163−176.
(44) Zhong, Y.; Feng, X.; Chen, W.; Wang, X.; Huang, K.; Gnanou, Y.; Lai, Z. Using UCST ionic liquid as a draw solute in forward osmosis to treat high-salinity water. *Environ. Sci. Technol.* **2016**, *50*, 1039−1045.
(45) Barradas, J. M.; Dida, B.; Matula, S.; Dolezal, F. A model to formulate nutritive solutions for fertigation with customized electrical conductivity and nutrient ratios. *Irrig. Sci.* **2018**, *36*, 133−142.
(46) Beg, M.; Clark, H. C. Chemistry of the trifluoromethyl group: part v. Infrared spectra of some phosphorus compounds containing CF3. *Can. J. Chem.* **1962**, *40*, 393−398.
(47) Damian Risberg, E.; Eriksson, L.; Mink, J.; Pettersson, L. G.; Skripkin, M. Y.; Sandström, M. Sulfur X-ray absorption and vibrational spectroscopic study of sulfur dioxide, sulfite, and sulfonate solutions and of the substituted sulfonate ions X3CSO3-(X = H, Cl, F). *Inorg. Chem.* **2007**, *46*, 8332−8348.
(48) Das, S. K.; Majhi, D.; Sahu, P. K.; Sarkar, M. Investigation of the influence of alkyl side chain length on the fluorescence response of C153 in a series of room temperature ionic liquids. *RSC Adv.* **2015**, *5*, 41585−41594.
(49) Tritt, T. M.Thermoelectric Materials: Principles, Structure, Properties, and Applications. In *Encyclopedia of Materials: Science and Technology*, Buschow, K. H. J., Cahn, R. W., Flemings, M. C., Ilschner, B., Kramer, E. J., Mahajan, S., Veyssière, P., Eds.; Elsevier: Oxford, 2002, pp 1−11.
(50) McCarthy, O. J.Encyclopedia of Dairy Sciences (Second Edition). *InMilk | Physical and Physico-Chemical Properties of Milk;*Fuquay, J. W., Ed.; Academic Press: San Diego, 2002, pp 467−477.
(51) Hogeveen, H.Encyclopedia of Dairy Sciences (Second Edition). In *MASTITIS THERAPY AND CONTROL | Automated Online Detection of Abnormal Milk;*Fuquay, J. W., Eds.; Academic Press: San Diego, 2011, pp 422−428.
(52) Ohno, H.ELECTROLYTES | Ionic Liquids☆. In *Reference Module in Chemistry, Molecular Sciences and Chemical Engineering*; Elsevier: Netherlands, 2013.
(53) Chen, M.; White, B. T.; Kasprzak, C. R.; Long, T. E. Advances in phosphonium-based ionic liquids and poly(ionic liquid)s as conductive materials. *Eur. Polym. J.* **2018**, *108*, 28−37.

https://doi.org/10.1021/acsomega.2c05279
ACS Omega 2022, 7, 41508−41518

(54) Huang, H.; Xie, R.New Osmosis Law and Theory: the New Formula that Replaces van't Hoff Osmotic Pressure Equation. *arXiv preprint arXiv:1201.09122*012.
(55) Szutkowski, K.; Kołodziejska, Ż.; Pietralik, Z.; Zhukov, I.; Skrzypczak, A.; Materna, K.; Kozak, M. Clear distinction between CAC and CMC revealed by high-resolution NMR diffusometry for a series of bis-imidazolium gemini surfactants in aqueous solutions. *RSC Adv.* **2018**, *8*, 38470−38482.
(56) Kamio, E.; Takenaka, A.; Takahashi, T.; Matsuyama, H. Fundamental investigation of osmolality, thermo-responsive phase diagram, and water-drawing ability of ionic-liquid-based draw solution for forward osmosis membrane process. *J. Membr. Sci.* **2019**, *570-571*, 93−102.
(57) Kamio, E.; Kurisu, H.; Takahashi, T.; Matsuoka, A.; Yoshioka, T.; Nakagawa, K.; Sun, Y.; Matsuyama, H. Effect of temperature on the osmotic behavior of LCST type ionic liquid solutions as draw solutions in the forward osmosis process. *Sep. Purif. Technol.* **2021**, *275*, No. 119164.
(58) Park, J.; Joo, H.; Noh, M.; Namkoong, Y.; Lee, S.; Jung, K. H.; Ahn, H. R.; Kim, S.; Lee, J.; Yoon, J. H.; Lee, Y. Systematic structure control of ammonium iodide salts as feasible UCST-type forward osmosis draw solutes for the treatment of wastewater. *J. Mater. Chem. A* **2018**, *6*, 1255−1265.
(59) Osváth, Z.; Iván, B. The dependence of the cloud point, clearing point, and hysteresis of poly (N-isopropylacrylamide) on experimental conditions: The need for standardization of thermoresponsive transition determinations. *Macromol. Chem. Phys.* **2017**, *218*, No. 1600470.
(60) Chen, L.; Zhao, C.; Duan, X.; Zhou, J.; Liu, M. Finely Tuning the Lower Critical Solution Temperature of Ionogels by Regulating the Polarity of Polymer Networks and Ionic Liquids. *CCS Chem.* **2022**, *4*, 1386−1396.
(61) Zeweldi, H. G.; Bendoy, A. P.; Park, M. J.; Shon, H. K.; Kim, H.; Johnson, E. M.; Kim, H.; Lee, S.; Chung, W.; Nisola, G. M. Tetrabutylammonium 2, 4, 6-trimethylbenzenesulfonate as an effective and regenerable thermo-responsive ionic liquid drawing agent in forward osmosis for seawater desalination. *Desalination* **2020**, *495*, No. 114635.
(62) Zeweldi, H. G.; Bendoy, A. P.; Park, M. J.; Shon, H. K.; Johnson, E. M.; Kim, H.; Kim, H.; Chung, W.; Nisola, G. M. Forward osmosis with direct contact membrane distillation using tetrabutylphosphonium p-toluenesulfonate as an effective and safe thermo-recyclable osmotic agent for seawater desalination. *Chemosphere* **2021**, *263*, No. 128070.
(63) Suh, C.; Lee, S. Modeling reverse draw solute flux in forward osmosis with external concentration polarization in both sides of the draw and feed solution. *J. Membr. Sci.* **2013**, *427*, 365−374.
(64) Haupt, A.; Marx, C.; Lerch, A. Modelling Forward Osmosis Treatment of Automobile Wastewaters. *Membranes* **2019**, *9*, 106.
(65) An, X.; Hu, Y.; Wang, N.; Zhou, Z.; Liu, Z. Continuous juice concentration by integrating forward osmosis with membrane distillation using potassium sorbate preservative as a draw solute. *J. Membr. Sci.* **2019**, *573*, 192−199.

https://doi.org/10.1021/acsomega.2c05279
ACS Omega 2022, 7, 41508−41518